# Observations of atmospheric $^{14}CO_2$ at Anmyeondo GAW station, Korea: Implications for fossil fuel $CO_2$ and emission ratios

Haeyoung Lee[1,2], Edward J. Dlugokencky[3], Jocelyn C Turnbull [4,5], Sepyo Lee[1], Scott J. Lehman[6], John B Miller[3], Gabrielle Petron[3,5], Jeongsik Lim[7,8], and Gang-Woong Lee[2], Sang-Sam Lee[1] and Young-San Park[1]

*Correspondence to Haeyoung Lee (leehy80@korea.kr)*

[1]National Institute of Meteorological Sciences, Jeju, 63568, Republic of Korea
[2]Atmospheric Chemistry Laboratory, Hankuk University of Foreign Studies, Gyeonggi-do, 17035, Republic of Korea
[3]NOAA, Global Monitoring Laboratory, Boulder, Colorado, USA
[4] National Isotope Center, GNS Science, Lower Hutt, New Zealand
[5]CIRES, University of Colorado, Boulder, Colorado, USA
[6]INSTAAR, University of Colorado, Boulder, Colorado, USA
[7]Korea Research Institute of Standard and Science, Daejeon, 34113, Republic of Korea
[8] University of Science and Technology, Daejeon, 34113, Republic of Korea

*Abstract. To understand Korea's carbon dioxide ($CO_2$) emissions and sinks as well as those of the surrounding region, we used 70 flask-air samples collected during May 2014 to August 2016 at Anmyeondo (AMY, 36.53° N, 126.32° E; 46 m a.s.l) World Meteorological Organization (WMO) Global Atmosphere Watch (GAW) station, located on the west coast of South Korea, for analysis of observed $^{14}C$ in atmospheric $CO_2$ as a tracer of fossil fuel $CO_2$ contribution ($C_{ff}$). Observed $^{14}C/C$ ratios in $CO_2$ (reported as $\Delta$ values) at AMY varied from -59.5 to 23.1‰ with the measurement uncertainty of ±1.8‰. The derived mean value $C_{ff}$ of (9.7±7.8) µmol mol$^{-1}$ (1$\sigma$) is greater than that found in earlier observations from Tae-Ahn Peninsula (TAP, 36.73° N, 126.13° E, 20 m a.s.l., 28 km away from AMY) of (4.4±5.7) µmol mol$^{-1}$ from 2004 to 2010. The enhancement above background of sulfur hexafluoride ($\Delta x(SF_6)$) and carbon monoxide ($\Delta x(CO)$) correlate strongly with $C_{ff}$ ($r > 0.7$) and appear to be good proxies for fossil fuel $CO_2$ at regional*

*and continental scales. Samples originating from the Asian continent had greater $\Delta x(CO):C_{ff}$ ($R_{CO}$) values, (29±8) to (36±2) nmol μmol$^{-1}$, than in Korean local air ((8±2) nmol μmol$^{-1}$). Air masses originating in China showed (1.6±0.4) to (2±0.1) times greater $R_{CO}$ than a bottom-up inventory suggesting that China's CO emissions are underestimated in the inventory while observed $R_{SF6}$ values are 2-3 times greater than inventories for both China and Korea. However, both $R_{CO}$ derived from inventories and observations have decreased relative to previous studies, indicating that combustion efficiency is increasing in both China and South Korea.*

## 1 Introduction

Carbon Dioxide ($CO_2$) is the principle cause of climate change in the industrial era, and is increasing in the atmosphere at (2.4±0.4) μmol mol$^{-1}$ a$^{-1}$ in a recent decade globally (where 0.4 is the standard deviation of annual growth rates; www.esrl.noaa.gov/gmd/ccgg/trends/, last access: 6 December 2019). This increase is by release of $CO_2$ from fossil fuel combustion that has been demonstrated through $^{14}C$ analysis of tree rings from the last two centuries (Stuiver and Quay, 1981; Suess, 1955; Tans et al., 1979). Atmospheric measurement program for the ratio $^{14}C/C$ in $CO_2$ was initiated in the 1950s and 1960s (Rafter and Fergusson, 1957; Nydal, 1996). Observed $^{14}C/C$ ratios are reported in Delta notation ($\Delta(^{14}CO_2)$) as fractionation-corrected permil (or ‰) deviations from the absolute radiocarbon standard (Stuiver and Polach, 1977). Many studies show that the variation of $\Delta(^{14}CO_2)$ is an unbiased and now widely used tracer for $CO_2$ emitted from fossil-fuel combustion (Levin et al., 2003; Turnbull et al., 2006; Graven et al., 2009; Van der Laan et al., 2010; Miller et al., 2012). Therefore measurements of $\Delta(^{14}CO_2)$ are

50 important to test the effectiveness of emission reduction strategies to mitigate the rapid
51 atmospheric $CO_2$ increase, since they can partition observed $CO_2$ enhancements, $\Delta x(CO_2)$, into
52 fossil fuel $CO_2$ ($C_{ff}$) and biological $CO_2$ ($C_{bio}$) components with high confidence (Turnbull et al.,
53 2006).

54 When trace gases are co-emitted with $C_{ff}$, correlations of their enhancements with $C_{ff}$ improve
55 understanding of the emission sources of both $C_{ff}$ and the co-emitted tracers. For example, CO
56 and $CH_4$ emission inventories are typically more uncertain than the fossil fuel $CO_2$ emission
57 inventory, since fossil fuel $CO_2$ emissions related to complete combustion are generally well
58 estimated while emissions related to incomplete combustion and agricultural activities are poorly
59 constrained (Kurokawa et al., 2013). Temporal changes in the observed emission ratio of a trace
60 gas to $C_{ff}$ can be used to examine emission trends in the trace gas (Tohijima et al., 2014).
61 Therefore the observed emission ratios of trace gases to $C_{ff}$ can be used to evaluate bottom-up
62 inventories of various trace gases (e.g., Miller et al., 2012). Here, we used two trace gases,
63 carbon monoxide (CO) and sulfur hexafluoride ($SF_6$) for this analysis. CO is produced along
64 with $CO_2$ during incomplete combustion of fossil fuels and biomass. CO enhancements above
65 background ($\Delta x(CO_2)$) correlate well with $C_{ff}$ and have been used as a fossil fuel tracer
66 (Zondervan and Meijer, 1996; Gamnitzer et al., 2006; Turnbull et al., 2011a; Turnbull et al.,
67 2011b; Tohijima et al., 2014). $SF_6$ is an entirely anthropogenic gas and is widely used as an arc
68 quencher in high-voltage electrical equipment (Geller et al., 1997). At regional to continental
69 scales, persistent small leaks to the atmosphere of $SF_6$ are typically co-located with fossil fuel
70 $CO_2$ sources and allow $SF_6$ to be used as an indirect $C_{ff}$ tracer, if the leaks are co-located with $C_{ff}$
71 emissions at the location and scale of interest (Turnbull et al., 2006; Rivier et al., 2006).

South Korea is a rapidly developing country with fast economic growth, and it is located next to China, which is the world's largest emitter of anthropogenic $CO_2$ (Boden et al., 2017; Janssens-Maenhout et al., 2017). The first $\Delta(^{14}CO_2)$ measurements in South Korea were reported by Turnbull et al. (2011a) based on air samples collected during October 2004 to March 2010 at Tae-Ahn Peninsula (TAP, 36.73° N, 126.13° E, 20 m a.s.l.). This study showed that observed $CO_2$ at this site was often influenced by Chinese emissions and the observed ratio of $\Delta x(CO):C_{ff}$ ($R_{CO}$) was greater than expected from bottom-up inventories. However South Korean $\Delta(^{14}CO_2)$ data are still limited and the ratio of the other trace gases to $C_{ff}$ barely discussed.

Here we use whole-air samples collected in glass flasks during May 2014 to August 2016 at Anmyeondo (AMY, 36.53° N, 126.32° E; 46 m a.s.l.) World Meteorological Organization (WMO) Global Atmosphere Watch (GAW) station, located on the west coast of South Korea and about 28 km SSE of TAP, where the first study was conducted. We decompose observed $CO_2$ enhancements into their fossil fuel and biological components at AMY to understand sources and sinks of $CO_2$. We also implemented cluster analysis using the NOAA Hybrid Single Particle Lagrangian Integrated Trajectory Model (HYSPLIT) to calculate back-trajectories for sample times and dates. Based on clusters of trajectories from specific regions, trace gas enhancement: $C_{ff}$ ratios and correlation coefficients were analyzed, especially focused on $SF_6$ and CO, to determine the potential of alternative proxies to $\Delta(^{14}CO_2)$. Finally we compared our $\Delta x(CO):C_{ff}$ ratio with ratios determined from bottom-up inventories (EDGARv4.3.2 and Korea's National Inventory Report in 2018) to evaluate reported CO emissions and how they've changed since 2010.

## 2. Materials and Methods

### 2.1 Sampling site and methods

The AMY GAW station is managed by the National Institute of Meteorological Sciences (NIMS) in the Korea Meteorological Administration (KMA). It has the longest record of continuous $CO_2$ measurement in South Korea, beginning in 1999. It is located on the west coast of Korea about 130 km southwest of the megacity of Seoul, whose population was 9.8 million in 2017. Semiconductor and other industries exist within a 100 km radius of the station. Also, the largest thermal power plants fired by coal and heavy oil in South Korea are within 35 km to the northeast and southeast of the station. The closest town, around 30 km to the east of AMY, is well known for its livestock industries. Local economic activities are related to agriculture, e.g., production of rice paddies, sweet potatoes, and onions, and the area is also known for its leisure opportunities that increase traffic and tourists in summer, indicating the complexity of greenhouse gas sources around AMY. On the other hand, air masses often arrive at AMY from the west and south, which is open to the Yellow Sea. Therefore AMY observes enhanced $CO_2$ compared to many other East Asian stations due not only to numerous local sources but also long-range transport of air-masses from the Asian continent (Lee et al., 2019).

Two pairs of flask-air samples (4 flasks total, 2 L, borosilicate glass with Teflon O-ring sealed stopcocks) were collected about weekly from a 40 m tall tower at AMY, regardless of wind direction and speed from May 2014 to August 2016, generally between 1400 to 1600 local time (Table S1) using a semi-automated portable sampler. A pair of flasks was flushed for 10 min at 5-6 L $min^{-1}$ then pressurized to 5.5 psig in less than 1 min. A second pair is collected shortly after the first (within 20 min). The portable sampler was checked for leaks after pressurizing by

observing the pressure gauge before closing the stopcocks. Batches of sampled flasks were shipped to Boulder, CO, USA every two months.

A total of 70 sets were collected and analyzed at the National Oceanic and Atmospheric Administration/Earth System Research Laboratory/Global Monitoring Division (NOAA/ESRL/GMD) for $CO_2$, CO, and $SF_6$ and for $\Delta(^{14}CO_2)$ by University of Colorado Boulder, Institute of Arctic and Alpine Research (INSTAAR). NOAA/ESRL/GMD analyzed $CO_2$ using a non-dispersive infrared analyzer, $SF_6$ using gas chromatography (GC) with electron capture detection, and CO by vacuum UV, resonance fluorescence. All analyzers were calibrated with the appropriate WMO mole fraction scales (WMO-X2007 scale for $CO_2$, WMO-X2014A scale for CO, and WMO-X2014 for $SF_6$; https://www.esrl.noaa.gov/gmd/ccl/, last access: 4 December 2019). The measurement and analysis methods for those gases are described in detail (http://www.esrl.noaa.gov/gmd/ccgg/behind_the_scenes/measurementlab.html, last access: 4 December 2019). Measurement uncertainties for $CO_2$ and $SF_6$ are reported as 68% confidential intervals. For $CO_2$, it is 0.07 μmol $mol^{-1}$ for all measurements used here. For $SF_6$, it is 0.04 pmol $mol^{-1}$. For CO, measurement uncertainty has not yet been formally evaluated, but is estimated at 1 nmol $mol^{-1}$ (68% confidence interval). All $CO_2$, $SF_6$ and CO data at AMY can be downloaded through ftp://aftp.cmdl.noaa.gov/data/trace_gases/. When we compare NOAA's $CO_2$ measurements from flask-air with quasi-continuous measurements by KMA at AMY, the difference was -0.11±2.32 μmol $mol^{-1}$ (mean±1 σ), close to GAW's compatibility goal for $CO_2$ (±0.1 ppm for Northern Hemisphere measurements, Lee et al., 2019).

The analysis methods for $\Delta(^{14}CO_2)$ are described by Lehman et al.(2013). Measurement repeatability of $\Delta(^{14}CO_2)$ in aliquots of whole air extracted from surveillance cylinders is 1.8‰

(1 σ), roughly equating to 1 μmol mol$^{-1}$ $C_{ff}$ detection capability from the measurement uncertainty alone. The $\Delta(^{14}CO_2)$ data at AMY was tabulated in Table S1. Among four flasks, the air from two flasks, after analysis for greenhouse gas mole fractions, was combined and analyzed for $\Delta(^{14}CO_2)$.

## 2.2 Data analysis method using $\Delta(^{14}CO_2)$ data

### 2.2.1 Calculation of $C_{ff}$ and $C_{bio}$

As Turnbull et al. (2009) suggested the observed $CO_2$ ($C_{obs}$) at AMY can be defined as:

$$C_{obs} = C_{bg} + C_{ff} + C_{other} \quad (1)$$

where $C_{bg}$, $C_{ff}$ and $C_{other}$ are the background, recently added fossil fuel $CO_2$ and the $CO_2$ derived from the other sources.

According to Tans et al. (1993), the product of $CO_2$ abundance and its isotopic ratio is conserved; the isotopic mass balance can be described as below:

$$\Delta_{obs}C_{obs} = \Delta_{bg}C_{bg} + \Delta_{ff}C_{ff} + \Delta_{other}C_{other} \quad (2)$$

where $\Delta$ is the $\Delta^{14}C$ of each $CO_2$ component of Equ. (1).

Therefore we can calculate fossil fuel $CO_2$ by combining equations (1) and (2) as:

$$C_{ff} = \frac{C_{bg}(\Delta_{obs} - \Delta_{bg})}{\Delta_{ff} - \Delta_{bg}} - \frac{C_{other}(\Delta_{other} - \Delta_{bg})}{\Delta_{ff} - \Delta_{bg}} \quad (3)$$

Fossil fuel derived $CO_2$ contains no $^{14}C$ because the half–life of $^{14}C$ is (5700±30) years (Godwin, 1962) while these fuels are hundreds of millions of years old. As we mentioned in the section 1, $\Delta(^{14}CO_2)$ is reported as a per mil (‰) deviation from the absolute radiocarbon reference standard corrected for fractionation and decay with a simplified form; $\Delta(^{14}C) \approx [(^{14}C/C)sample/(^{14}C/C)standard - 1]1000‰$. Therefore $\Delta_{ff}$ is set at -1000‰ (Stuiver and Pollach, 1977). Background values ($\Delta_{bg}$) in equations (1) to (3) are determined from measurements from background air collected at Niwot Ridge, Colorado, a high altitude site at a similar latitude as AMY (NWR, 40.05° N, 105.58° W, 3,526 m a.s.l.). Turnbull et al. (2011a) showed that the choice of background values did not significantly influence derived enhancements due to the large regional and local signal at TAP, 28 km from AMY. NWR $\Delta(^{14}CO_2)$ and other trace gas background values are selected using a flagging system to exclude polluted samples (Turnbull et al., 2007), and then fitted with a smooth curve following Thoning et al. (1989).

The second term of equation (3) is typically a small correction for the effect of other sources of $CO_2$ that have a $\Delta^{14}C$ differing by a small amount that of the atmospheric background, such as $CO_2$ from the 1) nuclear power industry, 2) oceans, 3) photosynthesis and 4) heterotrophic respiration.

1) The nuclear power industry produces $^{14}C$ that can influence the $C_{ff}$ calculation. South Korea has nuclear power plants along the east coast that may influence AMY air samples when air-masses originated from the eastern part of Korea (Figure 1). It is also possible that Chinese nuclear plants could influence some samples. Here we did not make any correction for this since most nuclear installations in this region are pressurized water reactors, which produce mainly $^{14}C$

177 in $CH_4$ rather than $CO_2$ (Graven and Gruber, 2011). 2) For the ocean, although there may also be
178 a small contribution from oceanic carbon exchange across the Yellow Sea, we consider this
179 effect small enough to ignore (Turnbull et al., 2011a). It was also demonstrated there is no
180 significant bias from the oceans including East China Sea (Song et al., 2018), even at coastal
181 sites in the Northern Hemisphere (Turnbull et al., 2009). Larger scale ocean exchange and also
182 stratospheric exchange affect both background and observed samples equally, so they can be
183 ignored in the calculations. 3) For the photosynthetic terms, $^{14}C$ in $CO_2$ accounts for natural
184 fractionation during uptake, so we also set this observed value the same as the background value.
185 4) Therefore we only consider heterotrophic respiration. For land regions, where most fossil fuel
186 emissions occur, heterotrophic respiration could be a main contributor to the second term of
187 equation (3) due to $^{14}C$ disequilibrium potentially. When this value is ignored, $C_{ff}$ would be
188 consistently underestimated (Palstra et al., 2008; Riley et al., 2008; Hsueh et al., 2007; Turnbull
189 et al., 2006). For this, corrections were estimated as (-0.2±0.1) μmol $mol^{-1}$ during winter and (-
190 0.5±0.2) μmol $mol^{-1}$ during summer (Turnbull et al., 2009; Turnbull et al., 2006).

191 $CO_2$ enhancements relative to baseline $CO_2$ are defined as $\Delta x(CO_2)$, with the excess signal of
192 $C_{obs}$ minus $C_{bg}$ in Equ.(1). Partitioning of $\Delta x(CO_2)$ into $C_{ff}$ and $C_{bio}$ is calculated simply from the
193 residual of the difference between observed $\Delta x(CO_2)$ and $C_{ff}$.

194 **2.2.2 The ratio of trace gas enhancement to $C_{ff}$ and its correlation**

195 To obtain the correlation coefficient (r) between $C_{ff}$ and other trace gas enhancements ($\Delta x(x) =$
196 $x_{obs} - x_{bg}$) and the ratio of any trace gas to $C_{ff}$ ($R_{gas}$), we use reduced major axis (RMA) regression
197 analysis (Sokal and Rohlf, 1981). The distributions of $R_{gas}$ are normally broad and non-Gaussian

198 and RMA analysis is a relatively robust method of calculating the slope of two variables that
199 show some causative relationship. Here, $x_{bg}$ was derived from NWR with the same method
200 described in section 2.2.1. The relevant equations are presented from Equ. S1 to Equ. S3. Results
201 for each species are given in Table 1.

202

203 **2.3 HYSPLIT cluster analysis**

204 HYSPLIT trajectories were run using Unified Model-Global Data Assimilation and Prediction
205 System (UM-GDAPS) weather data at 25 km by 25 km horizontal resolution to determine the
206 regions that influence air mass transport to AMY. A total of 70 air-parcel back-trajectories were
207 calculated for 72-h periods at 3-h intervals matching the time of each flask-air sample taken at
208 AMY from May 2014 to August 2016. We assign the sampling altitude as 500 m, since it was
209 demonstrated that HYSPLIT and other particle dispersion back-trajectory models (e.g.,
210 FLEXPART) are consistent at 500 m altitude (Li et al., 2014). Cluster analysis of the resulting
211 70 back-trajectories categorized six pathways through which air parcels arrive at AMY during
212 the time period of interest.
213 Among the calculated back-trajectories, 67% indicate air masses originating from the Asian
214 continent. Back-trajectories of continental background air (CB) originating in Russia and
215 Mongolia occurred 13% of the time. 23% of the trajectories originated and travelled through
216 northeast China (CN). The CN region includes Inner Mongolia and Liaoning, one of the most
217 populated regions in China with 43.9 million people in 2012. These CN air masses arrive in
218 South Korea after crossing through western North Korea. 17% of the trajectories are derived
219 from central eastern China around the Shandong area (CE). The CE region contains Shandianzi

(SDZ, 40.65° N, 117.12° E, 287 m a.s.l.) located next to the megacities of Beijing and Tianjin, which are some of China's highest $CO_2$ emitting regions (Gregg et al., 2008). 14% are Ocean Background (OB) derived from the East China Sea. Among them, a few of the trajectories passed over the eastern part of China (e.g., over Shanghai) with high altitude (~1000 m). Flow from South Korea also travels through heavily industrialized and/or metropolitan regions in South Korea (Korea Local, KL, 19%) and under stagnant conditions (Polluted Local region, PL, 14%). Some of the KL air-masses have also passed over the East Sea and Japan.

## 3. Results and discussions

### 3.1 Observed $\Delta(^{14}CO_2)$ and portioning of $CO_2$ into $C_{ff}$ and $C_{bio}$

AMY $\Delta(^{14}CO_2)$ values are almost always lower than those observed at NWR, which we consider to be broadly representative of background values for the mid-latitude Northern Hemisphere (Figure 2). NWR $\Delta(^{14}CO_2)$ , which is based on weekly air samples, was in the range 10.0 to 21.2 ‰, with an average (16.6±3)‰ (1σ, standard deviation) from May 2014 to August 2016. Waliguan (WLG, 36.28° N, 100.9° E, 3816 m a.s.l.), an Asian background GAW station in China, also showed similar $\Delta(^{14}CO_2)$ levels to NWR with an average of (17.1±6.8)‰ in 2015 (Niu et al., 2016, measurement uncertainty ±3‰, n=20). $\Delta(^{14}CO_2)$ at AMY varied from -59.5 to 23.1‰ and had a mean value of (-6.2±18.8)‰ (1σ, n=70) during the measurement period (Table S1). This was similar to results from observations at SDZ, which is located about 100 km

northeast of Beijing, in the range of -53.0 to 32.6‰ with an average (-6.8±21.1)‰ (1σ, n=32) during Sep 2014 to Dec 2015 (Niu et al., 2016).

Calculated $C_{ff}$ at AMY ranges between -0.05 and 32.7 μmol mol$^{-1}$ with an average of (9.7±7.8) μmol mol$^{-1}$ (1σ, n=70); high $C_{ff}$ was observed regardless of season (Figure 2 (a)). One negative $C_{ff}$ value of -0.05 μmol mol$^{-1}$ was estimated due to greater AMY $\Delta(^{14}CO_2)$ than NWR on July 30, 2014. Although negative $C_{ff}$ values are non-physical, this value is not significantly different from zero, and is reasonable given that this air originated from the OB sector. The range of $C_{ff}$ in the AMY samples is similar to that observed at TAP from 2004 to 2010 (-1.6 to 42.9 μmol mol$^{-1}$ $C_{ff}$), but $C_{ff}$ is on average about twice as high at AMY as in the 2004 to 2010 TAP samples (mean (4.4±5.7) μmol mol$^{-1}$, n=202) (Turnbull et al., 2011a). A more detailed comparison of results based on differences between samples derived from the Asian continent and Korea local air is provided in section 3.2.

Estimated $C_{bio}$, as defined in section 2.2.1, varied from -18.1 to 15.7 μmol mol$^{-1}$ (mean (0.9±5.8) μmol mol$^{-1}$) at AMY (Figure 2 (c)). $C_{bio}$ showed a strong seasonal cycle with the lowest values from July to September when photosynthetic drawdown is expected to be strongest, in good agreement with the previous TAP study (Turnbull et al., 2011a). Even though $C_{bio}$ was at times negative, mainly due to photosynthesis during summer, the largest positive $C_{bio}$ was also observed in summer.

The largest $C_{ff}$ by season was observed in order of winter (DJF, (11.3±7.6), n=14) > summer (JJA, (10.7±9.2), n=11) > spring (MAM, (8.6±8.0), n=22) > autumn (SON, (7.6±5.6), n=17) with

a unit of μmol mol$^{-1}$. When we consider only positive contributions of $C_{bio}$ samples, the order was summer ((4.6±4.0), n=14) > autumn ((4.1±2.5), n=9) > spring ((3.8±2.6), n=13) > winter ((3.4±2.5), n=11) with a unit of μmol mol$^{-1}$.

$C_{ff}$ in summer was nearly as high as in winter. This is because lower wind speeds are observed at AMY during summer (Lee et al., 2019). When we analyzed seasonal boundary layer height for each sample by UM-GDAPS, it also showed similar result that it was highest in winter (with a range from 150 m to 1100 m) and lowest in summer (with a range from 100 m to 500 m). This suggests that these high summer $C_{ff}$ values may reflect emission from local activities, which were described in section 2.1, more than in other seasons.

The highest $C_{bio}$ value was also observed in the summer, PL sector. PL sector showed that positive $C_{bio}$ correlates with $CH_4$, which is a tracer for agriculture when observed in TAP local air masses. Turnbull et al.(2011a) also showed similar results.

In winter, $C_{bio}$ was relatively lower than in other seasons while $C_{ff}$ was highest. During winter, AMY is mainly affected by long-range transport of air-masses from China due to the Siberian high (Lee et al., 2019). Therefore air samples were less affected by local activities in winter but $C_{bio}$ still contributed almost 23% to $\Delta x(CO_2)$. In the dry season (from October to March), forest fires, which contribute the largest portion of total $CO_2$ emissions from open fires at the national scale, are concentrated in northeastern and southern China (Yin et al., 2019). The highest CO was observed in winter ((449.1±244.1) nmol mol$^{-1}$ (1σ) in winter while (236.8±124.4) nmol mol$^{-1}$ (1σ) in summer), which also supports biomass burning and bio fuels as large contributors to observed $CO_2$ enhancements in winter. Turnbull et al. (2011a) also showed that 20-30% of

280 winter $CO_2$ enhancements at TAP were likely contributed by biofuel combustion, along with
281 plant, soil, human, and animal respiration.

282 Regardless of the source, we find that $C_{bio}$ contributes substantially to atmospheric $CO_2$
283 enhancements at AMY in air masses affected by local and long-range transport, so when only
284 $CO_2$ enhancements above background are compared to bottom-up inventories, it can make a bias
285 due to $C_{bio}$ contributions.

286

287 3.2 $C_{ff}$ **comparison between Korea Local and Asian Continent samples**

288 To more clearly identify samples originating from the Asian continent (trajectory clusters CB,
289 CN, CE, and OB) and Korea Local (trajectory cluster KL) after cluster analysis of the 70 sets of
290 measurements, we use wind speed data from the Automatic Weather System (AWS) installed at
291 the same level as the air sample inlet at AMY. Among the data from CB, CN, CE, OB, and KL,
292 when wind speed was less than 3 m/s, we assumed that those samples could be affected by local
293 pollution. PL was also ruled out since it was affected by local pollutions under the stagnant
294 condition. Therefore we use only 41 sets of observations for this analysis (Table 1).

295 $C_{ff}$ is highest in the order CE > CN > KL > CB > OB (Table 1). During the measurement period,
296 the averages from Asian continent (sectors CE and CN) were higher than KL without the
297 baseline sector (CB and OB). The calculated mean $C_{ff}$ using only CE, CN, CB and OB, which
298 sample substantial outflow from the Asian Continent, was (7.6±3.9) μmol $mol^{-1}$.

When we compared the KL samples ((8.6±5.3) μmol $mol^{-1}$) with those from Korea Local air-masses observed at TAP ((8.5±8.6) μmol $mol^{-1}$, n=58, Turnbull et al., 2011a), mean $C_{ff}$ was quite similar (Figure 3). However, when comparing the $C_{ff}$ values from CB air masses in this study and TAP far-field (from China) samples (n=144, Turnbull et al., 2011a), $C_{ff}$ almost doubled from (2.6±2.4) to (4.3±2.1) μmol $mol^{-1}$, even though they might be expected to have had similar air mass back-trajectories. We also compared the values at SDZ from 2009 to 2010 (Turnbull et al., 2011a) and in 2015 (Niu et al., 2016); they also increased, not only in the samples that were affected by Beijing and North China Plain (SDZ-BN), which are comparably polluted, but also in the samples that were affected by northeast China (SDZ-NE). For SDZ-BN samples, $C_{ff}$ increased from (10±1) to (16±7.6) μmol $mol^{-1}$ from 2009/2010 (n=32) to 2015 (n=32). The AMY samples from CE, which flow over Beijing, showed (11.2±8.3) μmol $mol^{-1}$ of $C_{ff}$ and were also slightly greater than the 2009 – 2010 SDZ-BN samples (Turnbull et al., 2011a). For SDZ-NE samples, $C_{ff}$ was (3±7) μmol $mol^{-1}$ in 2009 to 2010 and increased to (7.6±6.8) μmol $mol^{-1}$ in 2015. Since the SDZ-NE samples are affected by northeast China according to Turnbull et al. (2011a) and Niu et al. (2016), we also see CN that originated from northeast china (NE) and its mean value of $C_{ff}$ had increased around (10.6±6.9) μmol $mol^{-1}$ compared to those values in 2009 to 2010.

It has been suggested that inter-annual variability in observed mean $C_{ff}$ in South Korea could reflect changing fossil fuel $CO_2$ emissions, or could indicate inter-annual variability in the air mass trajectories of the (small) dataset of flask-air samples (Turnbull et al., 2011a). Even though

the growth rate of $C_{ff}$ emission has been decreasing slowly in East Asia since 2010 due to emission reduction policies (Labzovskii et al., 2019), reported emissions increased 16.7% in China and 1.8% in South Korea from 2010 to 2016 (Janssens-Maenhout et al., 2017). This is broadly consistent with the flat trend in observed $C_{ff}$ in KL air masses, and in the upward trend in $C_{ff}$ observed in air-masses flowing out from Asia. Therefore it is possible that AMY mean $C_{ff}$ increased relative to the earlier TAP observations due to increased fossil fuel emissions from the Asian continent.

On the other hand, those values from this study showed large variability with small sample numbers due to different sampling strategy, environment, and synoptic conditions such as boundary layer height at the sampling time from reference studies. Further study will be necessary to understand those increased values.

### 3.3. Correlation of $C_{ff}$ with $SF_6$ and its emission ratios

We calculated correlation coefficients (r from Equ. (S3)) between $SF_6$ and CO enhancements with $C_{ff}$ and their ratios from Equ. (S1) with the 50 samples that were described in section 3.2 including PL sector (n=9) and whose values are tabulated in Table 1.

The correlations of CO enhancements ($\Delta x$(CO)) with $C_{ff}$ were strong ($r > 0.7$) in all sectors except PL, while $SF_6$ enhancements ($\Delta x(SF_6)$) correlated strongly with $C_{ff}$ ($r > 0.8$) for CE and OB in outflow from the Asian Continent and KL. $R_{CO}$ and $R_{SF6}$ were different between Korea Local and outflows from the Asian Continent. Here we discuss $R_{SF6}$ and section 3.4 discuss $R_{CO}$ more detail.

For $SF_6$, observed mean levels were high in order of (KL, PL) > (CN, CE) > (OB, CB) (Table 1). $SF_6$ in KL and PL were higher than from the Asian Continent, since South Korea has larger $SF_6$ emissions than most countries (ranked at 4$^{th}$ as of 2010 according to the EDGAR4.2.) because of liquid-crystal display (LCD) and electrical equipment production (Fang et al., 2014). Even though both KL and PL showed higher $SF_6$ mole fraction than outflows of Asian Continent, the correlation is different between KL and PL (Table 1). Under stagnant conditions, emitted $SF_6$ is less diluted by mixing, so that in PL, $\Delta x(SF_6)$ correlated weakly with $C_{ff}$. On the other hand, KL, CE and OB showed strong correlations ($r > 0.8$). Those three sectors are also larger $SF_6$ sources compared to other regions, according to $SF_6$ emission estimates for Asia (Fang et al., 2014). Because long-range transport allows time for mixing, $SF_6$ and $C_{ff}$ emissions are effectively co-located at not only continental scales but also regional scales. Thus $SF_6$ can be a good tracer of fossil fuel $CO_2$ for those regions.

The correlation between $\Delta x(SF_6)$ and $C_{ff}$ was strong in CE, OB and KL, however, $R_{SF6}$ is different between South Korea and outflow from the Asian continent (Figure S2). In a previous study, observed $R_{SF6}$ was 0.02 to 0.03 pmol μmol$^{-1}$ at NWR in 2004 (Turnbull et al., 2006). Here, the ratio was at (0.19±0.03) and (0.17±0.03) pmol μmol$^{-1}$ for CE and OB respectively. For KL, it was (0.66±0.16) pmol μmol$^{-1}$ indicating much larger ratios than in outflow from the Asian continent. Further, observed $R_{SF6}$ is 2 to 3 times greater for all air masses than predicted from bottom-up inventories based on national scale roughly. For this calculation, we use EDGAR4.3.2 for $CO_2$ and EDGAR4.2 for $SF_6$. We repeat the calculations for both $CO_2$ and $SF_6$ with Korea's National Inventory Report (KNIR, Greenhouse Gas Inventory and Research Center, 2018). Using $SF_6$ for 2010 from EDGAR4.2, we obtain $R_{SF6}$ of 0.08 pmol μmol$^{-1}$ for China while for

South Korea it was 0.14 pmol μmol$^{-1}$. Especially for South Korea, this is much lower than the observed $R_{SF6.}$ When KL $R_{SF6}$ was compared to ratios calculated from the KNIR inventory (0.27 pmol μmol$^{-1}$ for 2010 and 0.22 pmol μmol$^{-1}$ for 2014), it was closer to observed $R_{SF6}$ than EDGAR, but still underestimated (Figure S3 and S2). This result suggests that the observed ratio could be used to re-evaluate the bottom-up inventories (Rivier et al., 2006), especially targeting the Asian continent. Even though KL $R_{SF6}$ showed greater uncertainty than CE and OB, it is still greater than bottom-up inventories, such as KNIR and EDGAR. Therefore it would be useful to get more data to try and derive a more robust estimate to evaluate $SF_6$ emission inventories for Korea.

### 3.4 Correlation of $C_{ff}$ with CO and its emission ratios

High CO was mainly observed in outflow from the Asian continent in order of CE > CN > PL > (CB, KL) > OB (Table 1). The order of CO is quite different to that of $SF_6$. CO from KL and PL is lower than from outflow from the Asian continent, except for the OB sector, indicating that high CO can be a tracer of outflow from the Asian continent. Since CO is produced during incomplete combustion of fossil fuel and biomass, it is more closely related to fossil fuel $CO_2$ emissions than the other trace gases. Therefore in most cases the correlation between CO and $C_{ff}$ was strong. $R_{CO}$ was very different between air masses originating from South Korea Local ((8±2) nmol μmol$^{-1}$) and the Asian continent ((29±8) to (36±2) nmol μmol$^{-1}$), due to differences in combustion efficiencies and the use of catalytic converters. The higher continental emission ratios may also result from some contribution of biofuel combustion and agricultural burning in the Asian continent, which have significantly higher CO emission than fossil-fuel combustion

(Akagi et al., 2011). For example, for CB the CO level is similar to KL while $R_{CO}$ is higher than KL with low $C_{ff}$.

Typically CO shows seasonal variations with lower values in summer due to the atmospheric chemical sink, OH. Among the samples, the samples collected in summer were mainly rejected through wind speed cut-off (less than 3 m/s) since AMY has lower wind speed in summer (Lee et al., 2019). Only OB sector includes 4 summer samples (of 7), because summer air masses are mainly from the southern part of the Yellow Sea (Lee et al., 2019). However, we assumed $R_{CO}$ is less affected by the summer sink, since only two $\Delta x$(CO) samples were negative for OB (Figure S1) and $R_{CO}$ was consistent whether or not the negative $\Delta x$(CO) values were considered. To compare emission ratios derived from atmospheric observations with those from inventories for 2000 to 2012, we calculated inventory emission ratio ($I_{CO/CO2}$) as:

$$I_{CO/CO2} = E_{CO}/E_{CO2} \times M_{CO2}/M_{CO}$$

Where, $E_{CO}$ and $E_{CO2}$ are total CO and fossil fuel $CO_2$ emissions in gigagrams (Gg, $10^9$ g) from the bottom-up national inventory. $M_X$ is the molar masses of CO and $CO_2$ in g $mol^{-1}$.

We use EDGAR4.3.2 (Janssens-Maenhout et al., 2017) and KNIR (Greenhouse Gas Inventory and Research Center, 2018) for inventory information for both CO and $CO_2$.

The uncertainty of EDGAR4.3.2 fossil fuel $CO_2$ emissions was reported as a 95% confidence interval (Janssens-Maenhout et al., 2019), ±5.4% for China and ±3.6% for South Korea (personal communication with Dr. Efisio Solazzo). The uncertainties of CO and $SF_6$ emissions were not reported by EDGAR. For KNIR, the $CO_2$ 2016 emission uncertainty in the energy

sector was ±3% (Greenhouse Gas Inventory and Research Center, 2018). KNIR does not provide uncertainties for other emission sectors of $CO_2$, nor from emissions of CO and $SF_6$.

In Fig. 4 we confirm that the CO to $C_{ff}$ emission ratios ($R_{CO}$) derived from both observations and inventories for China and South Korea are decreasing. Since $C_{ff}$ emissions appear to be flat (South Korea) or slightly increasing (China), this indicates that combustion efficiency and/or scrubbing of CO is improving.

For South Korea, EDGAR4.3.2 indicated that CO emissions from the energy sector (98% to 99% of total emission) decreased by 47% between the 1997 and 2012. South Korean fossil fuel $CO_2$ emissions increased until 2011 and remained mostly constant from 2011 to 2016 ((603,901±4,315) Gg $CO_2$) (Figure S4). Therefore the decreased trend in the emission ratio seems to reflect recent decreases in CO emissions in South Korea. Turnbull et al. (2011a) determined an observed mean $R_{CO}$ of (13±3) nmol μmol$^{-1}$ during 2004 to 2010. Suntharalingam et al. (2004) estimated $R_{CO}$ 15.4 nmol μmol$^{-1}$ for South Korea in 2001 from $CO_2$ and CO airborne observations ($C_{ff}$ was not determined). Recently, the KORUS-AQ campaign, which was conducted over Seoul from May to June in 2016, estimated $R_{CO}$ as 9 nmol μmol$^{-1}$ (Tang et al., 2018) based on $CO_2$ and CO observations ($C_{ff}$ was not determined). Our study gives $R_{CO}$ of (8±2) nmol μmol$^{-1}$ for South Korea, slightly but not significantly lower than the KORUS-AQ result for Seoul. Different contributions of $C_{bio}$ and $C_{ff}$ to total $CO_2$ may bias the $R_{CO}$ calculation when total $CO_2$ was used in the KORUS-AQ study (e.g., Miller et al., 2012). The South Korean national $R_{CO}$ from EDGAR4.3.2 in 2012 was 6.7 nmol μmol$^{-1}$, consistent with our observations. Using KNIR for 2016, we obtain $R_{CO}$ of 2.1 nmol μmol$^{-1}$. KNIR suffers from a large number of

missing CO emission sources compared to the EDGAR, as indicated by their reported emissions, 638.3 and 2580.8 Gg in 2012, respectively (Figure S5). For example, CO emissions recently derived from fugitive emissions and residential/other sectors increased to 14% and 11.5% of total emission respectively in EDGAR but were not reported in KNIR.

For China the inventories estimate that CO emissions from the energy sector, (96.5±0.2)%, were almost constant through the 1990s, and then increased during the early-2000s from industrial processes (8.8% of total emissions in 2012). Fossil fuel $CO_2$ emission in China also increased until 2013 and then stayed roughly constant at (10,461,890±60,571) Gg according to EDGAR4.3.2. Thus even though both emissions show an increase from 2000 to 2016 for fossil fuel $CO_2$ and to 2012 for CO, the emission ratio decreased (Figure S4 and Figure 4) seeming to indicate that combustion efficiency is improving. Many studies observed decreasing $R_{CO}$ in China from 2000 to 2010 (Turnbull et al., 2011a; Wang et al., 2010). Suntharalingam et al. (2004) reported $R_{CO}$ was 55 nmol μmol$^{-1}$ in 2001 ($C_{ff}$ was not determined). In the Beijing region, $R_{CO}$ decreased from 57.80 to 37.59 nmol μmol$^{-1}$ during 2004 to 2008 (Wang et al., 2010). The overall $R_{CO}$ was (47±2) nmol μmol$^{-1}$ at SDZ for 2009-2010 and (44±3) nmol μmol$^{-1}$ in air-masses that originated from the Asian continent from 2005 to 2009 (Turnbull et al., 2011a). Tohjima et al. (2014) explained that surface based $R_{CO}$ decreased from 45 to 30 nmol μmol$^{-1}$ in outflow air masses from China from 1998 to 2010. Fu et al. (2015) also observed $R_{CO}$ of 29 nmol μmol$^{-1}$ over mainland China in 2009. In Beijing, which is located along the path of CE, it was (30.4±1.6) nmol μmol$^{-1}$ and (29.6±3.2) nmol μmol$^{-1}$ for Xiamen in 2016, which is in the OB sector (Niu et al., 2018). During KORUS-AQ in 2016, $R_{CO}$ of 28 nmol μmol$^{-1}$ was observed over the Yellow

Sea. Some of those studies did not differentiate $C_{ff}$ from the total $CO_2$ enhancement, so, although $R_{CO}$ still includes uncertainties, it is continually decreasing.

In this study $R_{CO}$ is (29±8), (31±8), (36±2), and (31±4) nmol μmol$^{-1}$ for CB, CN, CE and OB, consistent with Tang et al.(2018) and Liu et al.(2018). On the other hand, $R_{CO}$ in CE is higher than in other sectors in this study. The Shandong area, which is located in the path of CE, has been plagued with problems of combustion inefficiency and ranked as the largest consumer of fossil fuels in all of China (Chen and Li, 2009). The uncertainties in our observed $R_{CO}$ for this region overlap with other sectors such as CB, CN and OB, so further monitoring of the ratios will help to get more detailed information.

In South Korea and China, atmosphere-based $R_{CO}$ values calculated by this study are (1.2±0.3) times (with KL), (1.6±0.4), (1.7±0.4), (2±0.1) and (1.7±0.2) times greater (with CB, CN, CE and OB) than in the inventory, respectively (Figure 4). This is in agreement with previous studies (Turnbull et al., 2011a; Kurokawa et al., 2013; Tohjima et al., 2014). One explanation is that EDGAR does not reflect secondary CO production, which can be a significant contributor to CO (Kurokawa et al., 2013). Also, CO derived from biomass burning and biofuels was not included in this inventory. Therefore, this indicates that top-down observations are necessary to evaluate and improve bottom-up emission products.

## 4. Summary and Conclusions

To understand $CO_2$ sources and sinks in Korea as well as those of the surrounded region, we collected $\Delta(^{14}CO_2)$ with 70 flask samples from May 2014 to August 2016. We summarized our results below.

1) Observed $\Delta(^{14}CO_2)$ values at AMY ranged from -59.5 to 23.1‰ (a mean value of (-6.2±18.8)‰ (1σ)) during the study period, almost always lower than those observed at NWR, which we consider to be broadly representative of background values for the mid-latitude Northern Hemisphere. This reflects the strong imprint of fossil fuel-$CO_2$ emissions recorded in AMY air samples.

2) Calculated $C_{ff}$ using $\Delta(^{14}CO_2)$ at AMY ranges between -0.05 and 32.7 μmol mol$^{-1}$ with an average of (9.7±7.8) μmol mol$^{-1}$ (1σ); this average is twice as high as in the 2004 to 2010 TAP samples (mean (4.4±5.7) μmol mol$^{-1}$) (Turnbull et al., 2011a). We also observed high $C_{ff}$ regardless of the season or source region. After separately identifying samples originating from the Asian continent and the Korean peninsula, we determined that the mean $C_{ff}$ increased relative to the earlier observations due to increased fossil fuel emissions from the Asian continent as showing by the consistent growth in reported emissions, which increased 16.7% in China and only 1.8% in South Korea from 2010 to 2016. Note, however, that our data span a relatively limited time period and are subject to different synoptic conditions during the sampling time from previous studies, so a longer time-series would increase confidence in tracking this change.

3) Because $\Delta x$(CO) and $\Delta x(SF_6)$ agreed well with $C_{ff}$, but showed different slopes for Korea and the Asian continent, those $R_{gas}$ values can be indicators of air mass origin and those

gases can be proxies for $C_{ff}$. Overall, we have confirmed that both $R_{CO}$ derived from inventory and observation have decreased relative to previous studies, indicating that combustion efficiency is increasing in both China and South Korea.

4) However, atmosphere-based $R_{gas}$ values are greater than bottom-up inventories. For CO, our values are (1.2±0.3) times and (1.6±0.4) to (2±0.1) times greater than in inventory values for South Korea and China, respectively. This discrepancy may arise from several sources including the absence of atmospheric chemical CO production such as oxidation of $CH_4$ and non-methane VOCs. Observed $R_{SF6}$ is 2 to 3 times greater than in inventories. Therefore those values in our study can be used for improving bottom-up inventories in the future.

5) Finally, we stress that because $C_{bio}$ contributes substantially to $\Delta x(CO_2)$, even in winter, $\Delta^{14}C$-based $C_{ff}$ (and not $\Delta x(CO_2)$) is required for accurate calculation of both $R_{CO}$ and $R_{SF6}$.

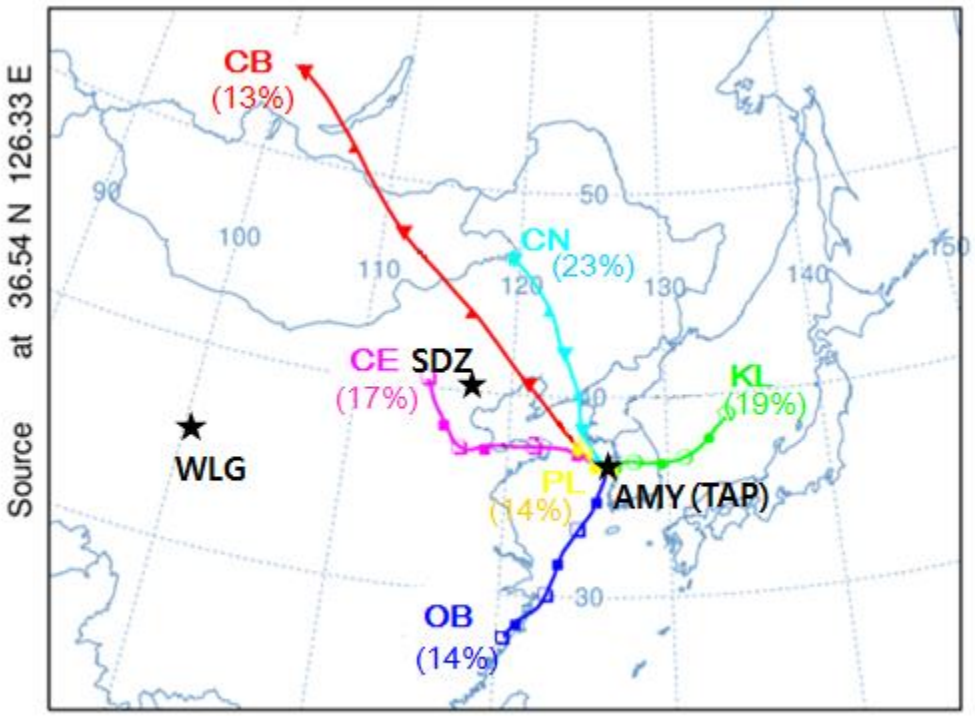


Figure 1. A total of 70 air-parcel back-trajectories were calculated for 72-h periods at 3-h intervals from May 2014 to August 2016 using the HYSPLIT model in conjunction with KMA UM GDAPS data at 25 km by 25 km resolution. Station locations are: WLG (Waliguan, 36.28° N, 100.9° E, 3816 m a.s.l.), SDZ (Shandianzi, 40.65° N, 117.12° E, 287 m a.s.l.), and AMY (Anmyeondo, 36.53° N, 126.32° E, 86 m a.s.l.). TAP (Tae-Ahn Peninsula, 36.73° N, 126.13° E, 20 m a.s.l.) is around 28 km northeast from AMY.

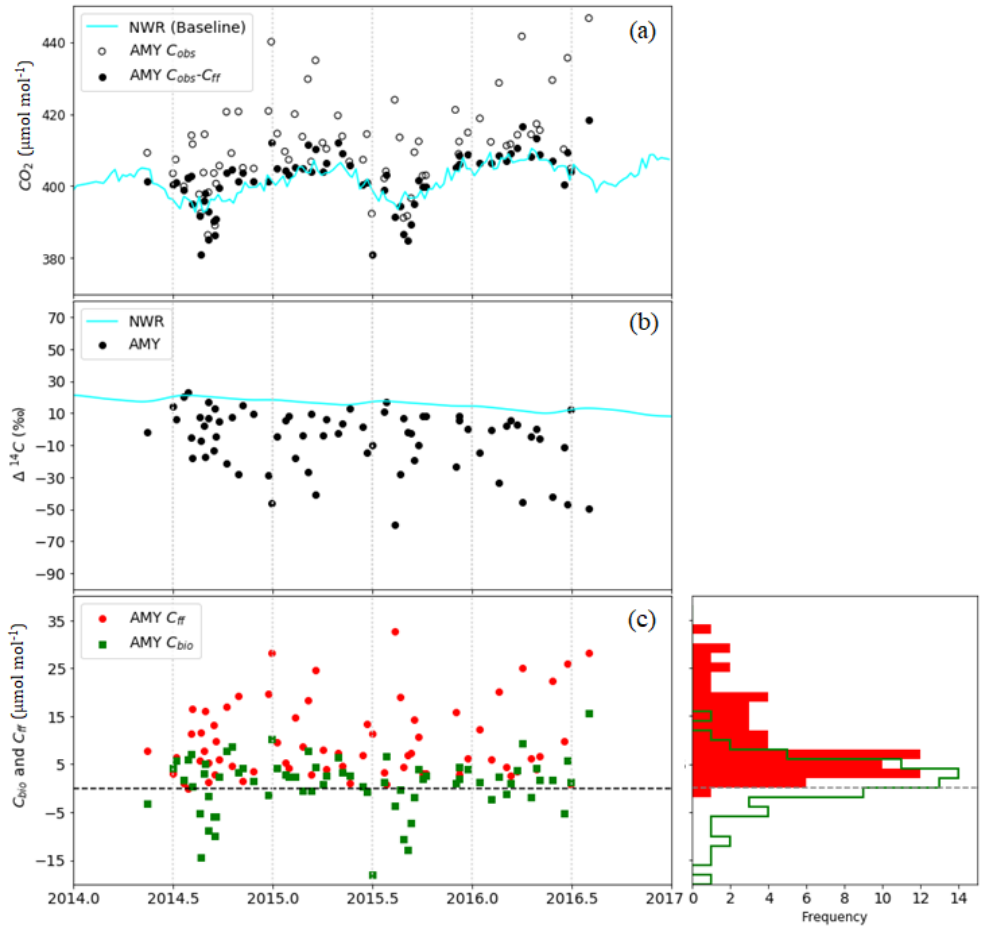


Figure 2. Time series of (a) observed $CO_2$ dry air mole fraction (open circles) and observed $CO_2$ ($C_{obs}$) minus $C_{ff}$ calculated from $\Delta(^{14}CO_2)$ (closed circles). (b) $\Delta(^{14}CO_2)$ at AMY (black circles) and at NWR (Niwot Ridge, line), baseline data. (c) Time series of $C_{ff}$ and $C_{bio}$ calculated from $\Delta(^{14}CO_2)$ (left) and the frequency distribution at AMY (right).

514

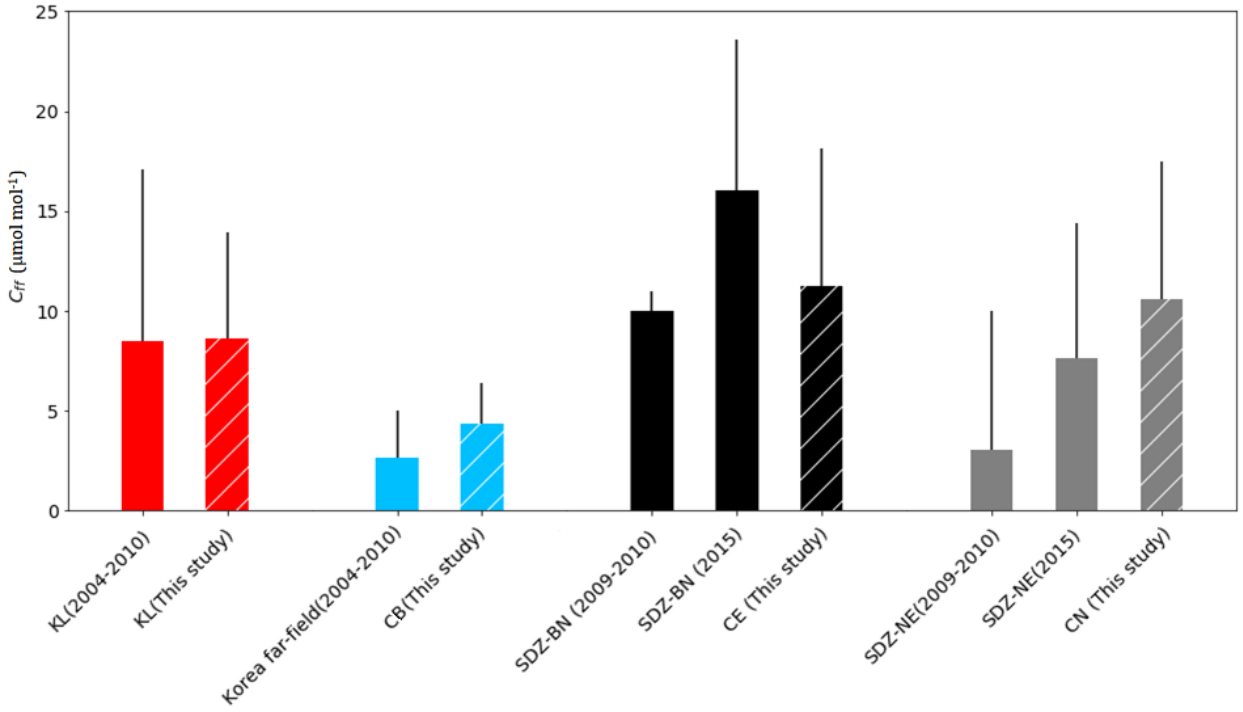


515

516 Figure 3. Calculated $C_{ff}$ (μmol mol$^{-1}$). Red bars are for KL and blue bars are for Korea far-field
517 (China) (2004-2010 from Turnbull et al. (2011a)). Black bars are for SDZ-BN samples that were
518 affected by Beijing and North China plain. Gray bars for SDZ-NE indicate samples that were
519 affected by regions northeast of SDZ. SDZ (2009-2010) is from Turnbull et al. (2011a) and SDZ
520 (2015) is from Niu et al. (2016). Hatched red, blue, black and grey bars are derived from this
521 study during 2014 to 2016.

(a) (b)

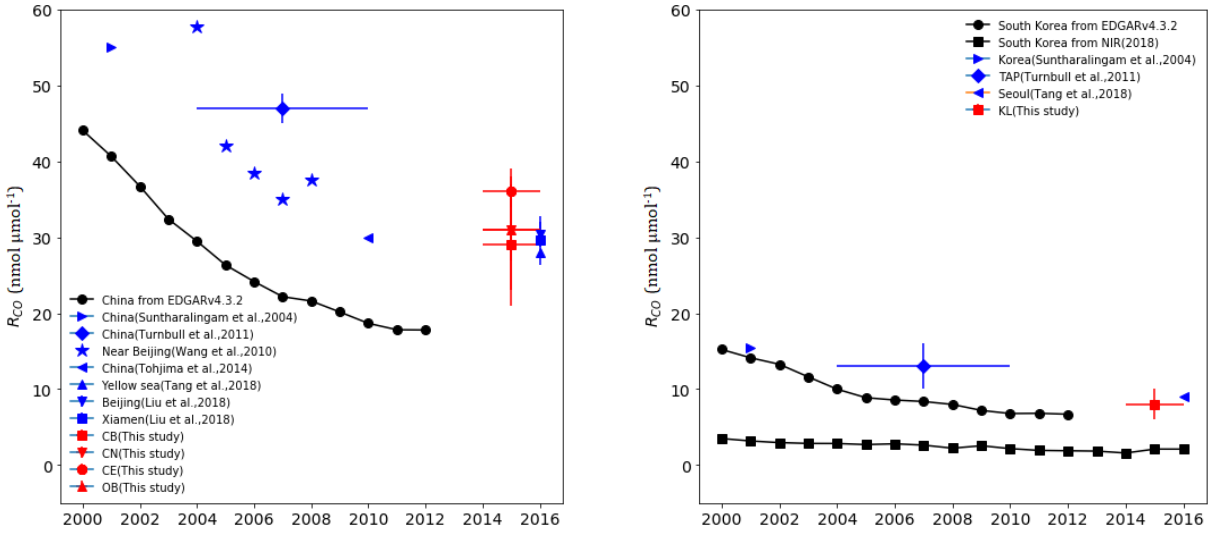


522 Figure 4. $R_{CO}$ for China (a) and for South Korea (b). Black circles: EDGARv.4.3.2 emission
523 inventory. Black squares: National Inventory Report, Korea (2018). Blue symbols are from other
524 studies (Suntharalingam et al., 2004; Wang et al., 2010; Turnbull et al., 2011a; Tohjima et al.,
525 2014; Liu et al., 2018; Tang et al., 2018). Red symbols: This study. Y-error bars: uncertainty in
526 the slope according to equation (S2). X-error bars: the period for the mean value.

527

Table 1. Means and standard deviations of $C_{ff}$ (μmol $mol^{-1}$), CO (nmol $mol^{-1}$) and $SF_6$ (pmol $mol^{-1}$) (total N=50, without PL N=41). The correlations (r) and the ratio ($R_{gas}$) of enhancement between $C_{ff}$ were determined by Reduced Major Axis (RMA) regression analysis on each scatter plot to obtain regression slopes. The uncertainty of $R_{gas}$ refers to equation (S2). When r is less than 0.7, $R_{gas}$ was not included here. N is the number of data. The unit of $R_{CO}$ is nmol $\mu mol^{-1}$ and for $R_{SF6}$ it is pmol $\mu mol^{-1}$. A plot of $R_{CO}$ and $R_{SF6}$ is shown in Figure S1.

| | Outflow from the Asia continent | | | | South Korea | |
|---|---|---|---|---|---|---|
| | CB (N=7) | CN (N =9) | CE (N =9) | OB (N =7) | KL (N =9) | PL (N =9) |
| $C_{ff}$ | 4.3±2.1 | 10.6±6.9 | 11.2±8.3 | 4.1±2.7 | 8.6±5.3 | 15.6±11.6 |
| CO | 233±59 | 353±219 | 473±293 | 169±90 | 228±40 | 259±100 |
| $SF_6$ | 9.0±0.4 | 10.1±1.2 | 10.1±1.5 | 9.2±0.5 | 13.0±3.3 | 12.7±6.2 |
| $R_{CO}$ (r) | 29±8 (0.80) | 31±8 (0.76) | 36±2 (0.98) | 31±4 (0.96) | 8±2 (0.74) | - (0.44) |
| $R_{SF6}$ (r) | - (0.63) | - (0.48) | 0.19±0.03 (0.91) | 0.17±0.03 (0.94) | 0.66±0.16 (0.76) | - (0.38) |

## Data availability

Our $CO_2$, CO, $SF_6$ data from AMY and NWR can be downloaded from ftp://aftp.cmdl.noaa.gov/data/trace_gases. $\Delta(^{14}CO_2)$ data are provided in the supplementary material of this paper.

## Author contributions

HL wrote this paper and analyzed all data. HL and GWL designed this study. EJD and JCT guided and reviewed this paper. SL collected samples and gave the information of the data at AMY. EJD, JCT, SJL, JBM, GP, and JL provided data and reviewed the manuscript. All authors contributed this work.

## ACKNOWLEDGMENT

This work was funded by the Korea Meteorological Administration Research and Development Program "Research and Development for KMA Weather, Climate, and Earth system Services– Development of Monitoring and Analysis Techniques for Atmospheric Composition in Korea" under Grant (1365003041).

## REFERENCES

Akagi, S. K., R. J. Yokelson, C. Wiedinmyer, M. J. Alvarado, J. S. Reid, T. Karl, J. D. Crounse, P. O. Wennberg: Emission factors for open and domestic biomass burning for use in atmospheric models, Atmos. Chem. Phys. 11, 4039-4027, doi:10.5194/acp-11-4039-2011, **2011**

Boden, T.A., G. Marland, and R.J. Andres: National $CO_2$ Emissions from Fossil-Fuel Burning, Cement Manufacture, and Gas Flaring: 1751-2014, Carbon Dioxide Information Analysis Center, Oak Ridge National Laboratory, U.S. Department of Energy, doi 10.3334/CDIAC/00001_V2017, **2017**

Chen, Y. Y. Li: Low-carbon economy and China's regional energy use research. *Jilin Univ. J. Soc. Sci. Ed*. *49*(2), 66-73, **2009**

Fang, X., R. L. Thompson, T. Saito, Y. Yokouchi, J. Kim, S. Li, K. R. Kim, S. Park, F. Graziosi, A. Stohl: Sulfur hexafluoride ($SF_6$) emissions in East Asia determined by inverse modeling. *Atmos. Chem. Phys*. *14*, 4779–4791, doi:10.5194/acp-14-4779-2014, **2014**

Fu, X. W., H. Zhang, C.-J. Lin, X. B. Feng, L. X. Zhou, S. X. Fang: Correlation slopes of GEM/CO, GEM/$CO_2$, and GEM/$CH_4$ and estimated mercury emissions in China, South Asia, the Indochinese Peninsula, and Central Asia derived from observations in northwestern and southwestern China. *Atmos. Chem. Phys*. *15*, 1013-1028, doi:10.5194/acp-15-1013-2015, **2015**

Gamnitzer, U., U. Karstens, B. Kromer, R. E. M. Neubert, H. Schroeder, I. Levin: Carbon monoxide: A quantitative tracer for fossil fuel $CO_2$?. *J. Geohys. Res., 111*, D22302, doi:10.1029/2005JD006966, **2006**

Geller, L. S., J. W. Elkins, J. M. Lobert, A. D. Clarke, D. F. Hurst, J. H. Butler, R. C. Myers: Tropospheric $SF_6$: Observed latitudinal distribution and trends, derived emissions and interhemispheric exchange time. *Geophys. Res. Lett*., *24*(6), 675–678, doi:10.1029/97GL00523, **1997**

578 Graven, H. D. N. Gruber: Continental-scale enrichment of atmospheric $^{14}CO_2$ from the nuclear
579 power industry: Potential impact on the estimation of fossil fuel-derived $CO_2$. *Atmos. Chem.*
580 *Phys. Discuss*. *11*, 14,583–14,605, doi:10.5194/acpd-11-14583-2011, **2011**

581 Graven, H. D., B. B. Stephens, T. P. Guilderson, T. L. Campos, D. S. Schimel, J. E. Campbell, R.
582 F. Keeling: Vertical profiles of biospheric and fossil fuel-derived $CO_2$ and fossil fuel $CO_2$:CO
583 ratios from airborne measurements of $^{14}C$, $CO_2$ and CO above Colorado, USA, *Tellus*, *61*, 536–
584 546, DOI:10.1111/j.1600-0889.2009.00421.x, **2009**

585 Gregg, J. S. R. J. Andres, G. Marland: China: Emissions pattern of the world leader in $CO_2$
586 emissions from fossil fuel consumption and cement production, *Geophys. Res. Lett*. *35*, L08806,
587 doi:10.1029/2007GL032887, **2008**

588 Greenhouse Gas Inventory and Research Center: National Greenhouse Gas Inventory Report of
589 Korea; National statistics-115018, 11-1480906-000002-10,
590 www.gir.go.kr/home/index.do?menuld=36 (in Korean), **2018**

591 Hsueh, D. Y., N. Y. Krakauer, J. T. Randerson, X. Xu, S. E. Trumbore, J. R. Southon: Regional
592 patterns of radiocarbon and fossil fuel derived $CO_2$ in surface air across North America, *Geophys.*
593 *Res. Lett., 34*, L02816, doi:10.1029/2006GL027032, **2007**

594 Janssens-Maenhout, G., M. Crippa, D. Guizzardi, M. Muntean, E. Schaaf, J.G.J. Olivier,
595 J.A.H.W. Peters, K.M. Schure: Fossil $CO_2$ and GHG emissions of all world countries, EUR
596 28766 EN, Publications Office of the European Union, Luxembourg, ISBN 978-92-79-73207-2,
597 doi:10.2760/709792, JRC107877, **2017**

598 Janssens-Maenhout, G.; M. Crippa, D. Guizzardi, M. Muntean, E. Schaaf, F. Dentener, P.
599 Bergamaschi, V. Pagliari, J. G. J. Olivier, J. A. H. W. Peters, J. A. van Aardenne, S. Monni, U.
600 Doering, A. M. R. Petrescu, E. Solazzo, G. D. Oreggioni: EDGAR v4.3.2 Global Atlas of the
601 three major greenhouse gas emissions for the period 1970–2012, *Earth Syst. Sci. Data*, *11*, 959–
602 1002, https://doi.org/10.5194/essd-11-959-2019, **2019**

603 Kurokawa, J., T. Ohara, T. Morikawa, S. Hanayama, G. Janssens-Maenhout, T. Fukui, K.
604 Kawashima, H. Akimoto: Emissions of air pollutants and greenhouse gases over Asian
605 regionsduring 2000–2008: Regional Emission inventory in ASia (REAS) version 2, *Atmos.*
606 *Chem. Phys. 13*, 11019–11058, doi:10.5194/acp-13-11019-2013, **2013**

607 Labzovskiia, L.D., H. W. L. Mak, S. T. Keneaa, J.-S. Rhee, A. Lashkari, S. Li, T.-Y. Goo, Y.-S.
608 Oh, Y.-H. Byun: What can we learn about effectiveness of carbon reduction policies from
609 interannual variability of fossil fuel $CO_2$ emissions in East Asia? *Environ. Sci. Policy*. *96*, 132-
610 140, https://doi.org/10.1016/j.envsci.2019.03.011, **2019**

611 Lee, H., S.-O. Han, S.-B. Ryoo, J.-S. Lee, G.-W. Lee: The measurement of atmospheric $CO_2$ at
612 KMA GAW regional stations, its characteristics, and comparisons with other East Asian sites.
613 *Atmos. Chem. Phys*. *19*, 2149–2163, doi.org/10.5194/acp-19-2149-2019, **2019**

614 Lehman, S.J., J. B. Miller, C. Wolak, J.R. Southon, P.P. Tans, S.A. Montzka, C. Sweeney, A. E.
615 Andrews, B.W. LaFranchi, T. P. Guilderson: Allocation of terrestrial carbon sources using $^{14}CO_2$:
616 methods, measurement, and modelling. *Radiocarbon. 55*(2–3):1484–95, **2013**

617 Le Quéré, C., R. M. Andrew, P. Friedlingstein, S. Sitch, J. Hauck, J. Pongratz, P. A. Pickers, J. I.
618 Korsbakken, G. P. Peters, J. G. Canadell, A. Arneth, V. K. Arora, L. Barbero, A. Bastos, L. Bopp,

F. Chevallier, L. P. Chini, P. Ciais, S. C. Doney, T. Gkritzalis, D. S. Goll, I. Harris, V. Haverd, F. M. Hoffman, M. Hoppema, R. A. Houghton, G. Hurtt, T. Ilyina, A. K. Jain, T. Johannessen, C. D. Jones, E. Kato, R. F. Keeling, K. K. Goldewijk, P. Landschützer, N. Lefèvre, S. Lienert, Z. Liu, D. Lombardozzi, N. Metzl, D. R. Munro, J. E. M. S. Nabel, S. Nakaoka, C. Neill, A. Olsen, T. Ono, P. Patra, A. Peregon, W. Peters, P. Peylin, B. Pfeil, D. Pierrot, B. Poulter, G. Rehder, L. Robertson, E.M. Rocher, C. Rödenbeck, U. Schuster, J. Schwinger, R. Séférian, I. Skjelvan, T. Steinhoff, A. Sutton, P. P. Tans, H. Tian, B. Tilbrook, F. N. Tubiello, I. T. vander Laan-Luijkx, G. R. vander Werf, N. Viovy, A. P. Walker, A.J. Wiltshire, R. Wright, S. Zaehle, Bo. Zheng: Global Carbon Budget 2018. *Earth Syst. Sci. Data*. 10, 2141–2194, https://doi.org/10.5194/essd-10-2141-2018, **2018**

Levin, I., B., M. S. Kromer, H. Sartorius: A novel approach for independent budgeting of fossil fuel $CO_2$ over Europe by $^{14}CO_2$ observations, *Geophys. Res. Lett.* 30(23), 2194, doi:10.1029/2003GL018477, **2003**

Li, S., J. Kim, S. Park, S.-K. Kim, M.-K. Park, J. Mühle, G.-W. Lee, M. Lee, C. O. Jo, K.-R. Kim: Source identification and apportionment of halogenated compounds observed at a remote site in East Asia. *Eviron. Sci.Technol*. 48, 491−498, doi.org/10.1021/es402776w, **2014**

Miller, J.B., S. J. Lehman, S. A. Montzka, C. Sweeney, B. R. Miller, A. Karion, C. Wolak, E. J. Dlugokencky, J. Southon, J. C. Turnbull, P.P. Tans: Linking emissions of fossil fuel $CO_2$ and other anthropogenic trace gases using atmospheric $^{14}CO_2$. *J.Geophys.Res*. *117*, D08302, doi:10.1029/2011JD017048, **2012**

Niu, Z., W. Zhou, X. Feng, T. Feng, S. Wu, P. Cheng, X. Lu, H. Du, X. Xiong, Y. Fu: Atmospheric fossil fuel $CO_2$ traced by $^{14}CO_2$ and air quality index pollutant observations in

641 Beijing and Xiamen, China. *Environ. Sci. Pollut. Res*. *25*, 17109–17117,
642 doi.org/10.1007/s11356-018-1616-z, **2018**

643 Niu, Z., W. Zhou, P. Cheng, S. Wu, X. Lu, X. Xiong, H. Du, Y. Fu: Observations of atmospheric
644 $\Delta^{14}CO_2$ at the global and regional background sites in China: Implication for fossil fuel $CO_2$
645 inputs. *Eviron. Sci.Technol*. 50, 12122−12128 DOI: 10.1021/acs.est.6b02814, **2016**

646 Nydal, R., and K. Lövseth, Carbon-14 measurements in atmospheric $CO_2$ from Northern and
647 Southern Hemisphere sites, 1962–1993, technical report, *Carbon Dioxide Inf. Anal. Cent., Oak*
648 *Ridge Natl. Lab*., U.S. Dep. of Energy, Oak Ridge, Tenn, **1996**

649 Rafter, T. A., and G. J. Fergusson, "Atom Bomb Effect"—Recent increase of Carbon-14 content
650 of the atmosphere and biosphere, *Science*, 126(3273), 557–558, **1957**

651 Palstra, S. W., U. Karstens, H.-J. Streurman, H. A. J. Meijer: Wine ethanol $^{14}C$ as a tracer for
652 fossil fuel $CO_2$ emissions in Europe: Measurements and model comparison, *J. Geophys. Res*.,
653 *113*, D21305, doi:10.1029/2008JD010282, **2008**

654 Riley, W. G., D. Y. Hsueh, J. T. Randerson, M. L. Fischer, J. Hatch, D. E. Pataki, W. Wang, M.
655 L. Goulden: Where do fossil fuel carbon dioxide emissions from California go? An analysis
656 based on radiocarbon observations and an atmospheric transport model, *J. Geophys. Res.*, *113*,
657 G04002, doi:10.1029/2007JG000625, **2008**

658 Rivier, L., P. Ciais, D. A. Hauglustaine, P. Bakwin, P. Bousquet, P. Peylin, A. Klonecki:
659 Evaluation of $SF_6$, $C_2Cl_4$, and CO to approximate fossil fuel $CO_2$ in the Northern Hemisphere
660 using a chemistry transport model. *J. Geophys. Res*. 111, D16311, doi:10.1029/2005JD006725,
661 **2006**

662 Suntharalingam, P., D. J. Jacob, P. I. Palmer, J. A. Logan, R.M. Yantosca, Y. Xiao, M. J. Evans:
663 Improved quantification of Chinese carbon fluxes using $CO_2$/CO correlations in Asian outflow, *J.*
664 *Geophys. Res*. 109, D18S18, doi:10.1029/2003JD004362, **2004**

665 Suess, H. E. Radiocarbon concentration in modern wood, *Science*, 122,415, **1955**

666 Stuiver, M., P. Quay: Atmospheric $^{14}C$ changes resulting from fossil fuel $CO_2$ release and cosmic
667 ray flux variability*, Earth Planet. Sci. Lett*. *53*, 349–362, **1981**
668 Tang, W., A. F. Arellano, J. P. DiGangi, Y. Choi, G. S. Diskin, A. Agustí-Panareda, M.
669 Parrington, S. Massart, B. Gaubert, Y. Lee, D. Kim, J. Jung, J. Hong, J.-W. Hong, Y. Kanaya, M.
670 Lee, R. M. Stauffer, A. M. Thompson, J. H. Flynn, J.-H. Woo: Evaluating high-resolution
671 forecasts of atmospheric CO and $CO_2$ from a global prediction system during KORUS-AQ field
672 campaign. *Atmos. Chem. Phys*. *18*, 11007–11030, doi.org/10.5194/acp-18-11007-2018, **2018**

673 Tans, P. P.; J. A. Berry, R. F. Keeling: Oceanic$^{13}C/^{12}C$ observations: A new window on ocean
674 $CO_2$ uptake. *Global Biogeochem. Cycles. 7(2)*, 353–368, doi:10.1029/93GB00053, **1993**

675 Sokal, R. R., and F. J. Rohlf. 1981. Biometry. 2nd edition. Freeman, NY.

676 Song Jinming, Baoxiao Qu, Xuegang Li, Huamao Yuan, Ning Li, Liqin Duan: Carbon
677 sinks/sources in the Yellow and East China Seas-Air-sea interface exchange, dissolution in
678 seawater, and burial in sediments. *Science China Earth Sciences*. 61, 1583-1593, **2018**

679 Stuiver, M., Polach H. A. Discussion: Reporting of $^{14}C$ data, *Radiocarbon*, 19(3), 355–363, **1977**

680 Tans, P.P., A.F.M. de Jong, W.G. Mook: Natural atmospheric $^{14}C$ variation and the Suess effect,
681 *Science*, *280*, 826-828, **1979**

682 Thoning, K. W., P. P. Tans, W. D. Komhyr: Atmospheric Carbon dioxide at Mauna Loa
683 Observatory 2. Analysis of the NOAA GMCC Data, 1984–1985, *J. Geophys. Res*. *94*, 8549–
684 8565, **1989**

685 Tohjima, Y., M. Kubo, C. Minejima, H. Mukai, H. Tanimoto, A. Ganshin, S. Maksyutov, K.
686 Katsumata, T. Machida, K. Kita: Temporal changes in the emissions of $CH_4$ and CO from China
687 estimated from $CH_4/CO_2$ and $CO/CO_2$ correlations observed at Hateruma Island. *Atmos. Chem.*
688 *Phys. 14*, 1663–1677, doi:10.5194/acp-14-1663-2014, **2014**

689 Turnbull, J., P. Rayner, J. Miller, T. Naegler, P. Ciais, A. Cozic: On the use of $^{14}CO_2$ as a tracer
690 for fossil fuel $CO_2$: Quantifying uncertainties using an atmospheric transport model, *J. Geophys.*
691 *Res. 114*, D22302, doi:10.1029/2009JD012308, **2009**

692 Turnbull, J. C., S. J. Lehman, J. B. Miller, R. J. Sparks, J. R. Southon, P. P. Tans: A new high
693 precision $^{14}CO_2$ time series for North American continental air. *J. Geophys. Res. 112*, D11310,
694 doi:10.1029/2006JD008184, **2007**

695 Turnbull, J. C., P. P. Tans, S. J. Lehman, D. Baker, T. J. Conway, Y. S. Chung, J. Gregg, J. B.
696 Miller, J. R. Southon, L.-X. Zhou: Atmospheric observations of carbon monoxide and fossil fuel
697 $CO_2$ emissions from East Asia. *J. Geophys. Res., 116*, D24306,doi:10.1029/2011JD016691,
698 **2011a**

699 Turnbull, J. C., A. Karion, M. L. Fischer, I. Faloona, T. Guilderson, S. J. Lehman, B. R. Miller, J.
700 B. Miller, S. Montzka, T. Sherwood, S. Saripalli, C. Sweeney, P. P. Tans: Assessment of fossil
701 fuel carbon dioxide and other anthropogenic trace gas emissions from airborne measurements

over Sacramento, California in spring 2009, *Atmos. Chem. Phys*. *11(2)*, 705–721, doi:10.5194/acp-11-705-2011, **2011b**

Turnbull, J. C. J. B. Miller, S. J. Lehman, P. P. Tans, R. J. Sparks, J. Southon: Comparison of $^{14}CO_2$, CO, and $SF_6$ as tracers for recently added fossil fuel $CO_2$ in the atmosphere and implications for biological $CO_2$ exchange, *Geophys. Res. Lett., 33*, L01817, doi:10.1029/2005GL024213, **2006**

Van Der Laan, S, U. Karstens, R.E.M . Neubert, I.T. Van Der Laan-Luijkx and H.A.J. Meijer: Observation-based estimates of fossil fuel-derived $CO_2$ emissions in the Netherlands using $\Delta^{14}C$, CO and $^{222}$Radon, *Tellus B: Chemical and Physical Meteorology*, 62:5, 389-402, DOI:10.1111/j.1600-0889.2010.00493.x. **2010**

Wang, Y. J. W. Munger, S. Xu, M. B. McElroy, J. Hao, C. Nielsen, H. Ma: $CO_2$ and its correlation with CO at a rural site near Beijing: Implications for combustion efficiency in China, *Atmos. Chem. Phys*. 10, 8881–8897, doi:10.5194/acp-10-8881-2010, **2010**

Yin, L., P. Du, M. Zhang, M. Liu, T. Xu, Y. Song: Estimation of emissions from biomass burning in China (2003–2017) based on MODIS fire radiative energy data, *Biogeosciences,* 16, 1629–1640. **2019**

Zondervan, A., and Meijer, H. A. J: Isotopic characterization of $CO_2$ sources during regional pollution events using isotopic and radiocarbon analysis, *Tellus B: Chemical and Physical Meteorology*, 48(4), 601–612, doi:10.1034/j.1600-0889.1996.00013.x, **1996**